CONDENSED MATTER PHYSICS

Superionicity, disorder, and bandgap closure in dense hydrogen chloride

Jack Binns[1†], Andreas Hermann[2*], Miriam Peña-Alvarez[2], Mary-Ellen Donnelly[1], Mengnan Wang[1], Saori Imada Kawaguchi[3], Eugene Gregoryanz[1,4,2], Ross T. Howie[1], Philip Dalladay-Simpson[1*]

Hydrogen bond networks play a crucial role in biomolecules and molecular materials such as ices. How these networks react to pressure directs their properties at extreme conditions. We have studied one of the simplest hydrogen bond formers, hydrogen chloride, from crystallization to metallization, covering a pressure range of more than 2.5 million atmospheres. Following hydrogen bond symmetrization, we identify a previously unknown phase by the appearance of new Raman modes and changes to x-ray diffraction patterns that contradict previous predictions. On further compression, a broad Raman band supersedes the well-defined excitations of phase V, despite retaining a crystalline chlorine substructure. We propose that this mode has its origin in proton (H^+) mobility and disorder. Above 100 GPa, the optical bandgap closes linearly with extrapolated metallization at 240(10) GPa. Our findings suggest that proton dynamics can drive changes in these networks even at very high densities.

INTRODUCTION

Hydrogen bond networks are defined by the interactions between donor and acceptor atoms, epitomized in the ice rules governing the structure of water ice. The responses of these interactions to changes in temperature or pressure are critical to understand the physical properties of molecular crystals (*1*–*5*). Hydrogen bonds have been observed to rearrange, amorphize, and symmetrize under compression, leading to the extensive polymorphism defining the phase diagrams of simple molecules such as H_2O, H_2S, and NH_3 (*6*–*16*). The behavior of hydrogen bond networks at very high densities, beyond symmetrization, is not well explored except in computational predictions and is difficult to generalize. Water ice is suggested to transform to an orthorhombic structure that retains symmetric hydrogen bonds (*17*) before further transitions, including metallization, are predicted to lower the network symmetry in the terapascal pressure regime (*18*–*20*). The extensive icy mantles of Neptune, Uranus, and their exoplanet analogs experience pressures above the known symmetrization pressure of pure H_2O ($P \approx 90$ GPa), making this the dominant hydrogen-bonding regime beyond Earth (*21*–*24*).

Due to their comparatively weak hydrogen bonding, the hydrogen halides (H*X*, *X* = F, Cl, Br, and I) form solid phases characterized by disorder of the hydrogen atoms. In their lowest-density forms, hydrogen atoms are free to rotate about the halide centers of mass. When cooled and/or compressed, H*X* molecules form zigzagging chains with the underlying face-centered cubic (fcc) packing of the halide atom positions remaining essentially unchanged (*25*–*28*). The heavier hydrogen halides HBr and HI decompose under increasing pressure into their constituent elements at 39 and 11 GPa, respectively (*29*, *30*). However, previous studies of hydrogen chloride (HCl) indicate that decomposition should occur at much higher pressures (*31*, *32*), making it ideal for the study of a weakly constrained hydrogen-bonded system in the regime beyond symmetrization.

Prior work on compressed HCl has been limited to Raman and Brillouin spectroscopy measurements to 60 and 4.5 GPa, respectively (*32*, *33*); no diffraction studies at high pressure have been carried out to date. The structure of low-temperature/high-pressure phase III was determined by neutron diffraction (space group $Cmc2_1$) (*25*). Raman spectroscopy indicates that at room temperature, HCl phase I transforms to phase III at 19 GPa (*31*) before a further change to a phase IV with symmetrized hydrogen bonds at 51 GPa. The onset of symmetrization was inferred from the weakening and eventual disappearance of H—Cl stretching modes, implying that H atoms occupy positions in the center of Cl—H—Cl bonds. In doing so, the space group symmetry of the crystal is transformed to *Cmcm* (*29*, *31*). Density functional theory (DFT) calculations have been applied to predict the behavior of HCl at high densities. Structure-searching methods suggest a sequence of low-symmetry phases dominated by zigzag chains of symmetric hydrogen bonds: a triclinic $P\bar{1}$ structure above 108 GPa (*34*), a monoclinic $P2_1/m$ phase more stable than phase IV above 233 GPa (*35*), and another monoclinic $C2/m$ phase more stable than $P\bar{1}$ above 250 GPa (*36*).

Here, we combine experimental measurements and first-principles calculations to study HCl up to 256(10) GPa, more than four times the pressure limit of previous experiments. Our Raman spectroscopy measurements extend to 205(10) GPa above which the signal decays. X-ray diffraction patterns were collected up to 190(10) GPa. Visual and near-infrared (IR) optical transmission measurements could be performed up to 207(10) GPa at which point no transmission was measurable. Visual observation and microphotography demonstrate increased reflectivity suggestive of metallic behavior starting from ca. 220(10) GPa to 256(10) GPa, the highest pressure reached in this study. Our measurements confirm the structural transitions coinciding with hydrogen bond order (I to III) and inferred symmetrization (III and IV) reported previously (*31*, *32*). Phase IV is found to be stable up to 80(10) GPa. Above this pressure, phase V is identified by the appearance of new Raman modes accompanying subtle changes in diffraction patterns. Calculations indicate that

[1]Center for High Pressure Science & Technology Advanced Research, 1690 Cailun Rd, Pudong, Shanghai 201203, China. [2]School of Physics and Centre for Science at Extreme Conditions, University of Edinburgh, Edinburgh EH9 3JZ, UK. [3]Japan Synchrotron Radiation Research Institute (JASRI), Sayo, Hyogo 679-5198, Japan. [4]Key Laboratory of Materials Physics, Institute of Solid State Physics, Chinese Academy of Sciences, Hefei, China.
*Corresponding author. Email: philip.dalladay-simpson@hpstar.ac.cn (P.D.-S.); a.hermann@ed.ac.uk (A.H.)
†Present address: School of Science, RMIT University, Melbourne, Victoria 3000, Australia.

this transition reintroduces dynamic disorder as protons become mobile, hopping to new lattice sites. Upon further compression, a broad low-frequency feature emerges above 90(10) GPa, which, from our calculations, is found to be correlated to the gradual inhibition of the proton mobility. At 170(10) GPa, despite no substantial changes in the diffraction, the pressure-dependent behavior of this excitation changes, and HCl exhibits a closing bandgap, increased reflectivity, and intraband absorption, suggesting the presence of free charge carriers.

RESULTS AND DISCUSSION

HCl appears as a transparent liquid at room temperature, from which crystals of phase I nucleate after pressure was increased above 0.7 GPa. Phase I is characterized by Cl atoms forming an fcc lattice. Hydrogen atoms are free to rotate unhindered about the Cl atoms, and this isotropic state gives rise to a characteristic single Raman vibrational mode (vibron) (Fig. 1A) (*32*). This rotator phase was stable up to 18.1 GPa above which transition to phase III occurred, marked by the appearance of eight additional Raman modes. The relatively large stability range of phase I is a testament to the weak hydrogen bonding present in HCl. By comparison, the rotator phase of NH_3 orders at 3 to 4 GPa (*37*) and is absent in H_2O. X-ray diffraction patterns of phase III (Fig. 2) could be indexed to a *C*-centered orthorhombic unit cell $a = 4.5433(5)$, $b = 4.2822(5)$, and $c = 4.4404(5)$ Å at 19.3 GPa, space group $Cmc2_1$. The structure of phase III is characterized by zigzagging chains of HCl molecules with ordered hydrogen atoms in asymmetric Cl···H—Cl hydrogen bonds (*25*).

With increasing pressure, the hydrogen bonds in phase III shorten, eventually leading to an equalization of interatomic distances between the H atom and the neighboring donor and acceptor Cl atoms (Cl···H···Cl) (fig. S1). This change is detected in Raman spectroscopy measurements that show the softening and eventual loss of the HCl stretching mode at pressures above 51 GPa (Fig. 1). This continuous transition results in the symmetric hydrogen bond network that distinguishes phase IV and increases the space group symmetry to *Cmcm* (*31*, *32*). X-ray diffraction measurements cannot directly corroborate the phase III to IV transition due to the low scattering power of hydrogen. However, no changes were observed in diffraction patterns before or after this transition, confirming that the phase transformation is due to changes in hydrogen atom positions only. A secondary indication is provided by a distinct change in the linear compressibilities with pressure, which decreases due to the symmetrization (fig. S2). Our own calculations confirm the hydrogen bond symmetrization transition at 50(3) GPa (fig. S1), and unit cell dimensions derived from DFT calculations show excellent

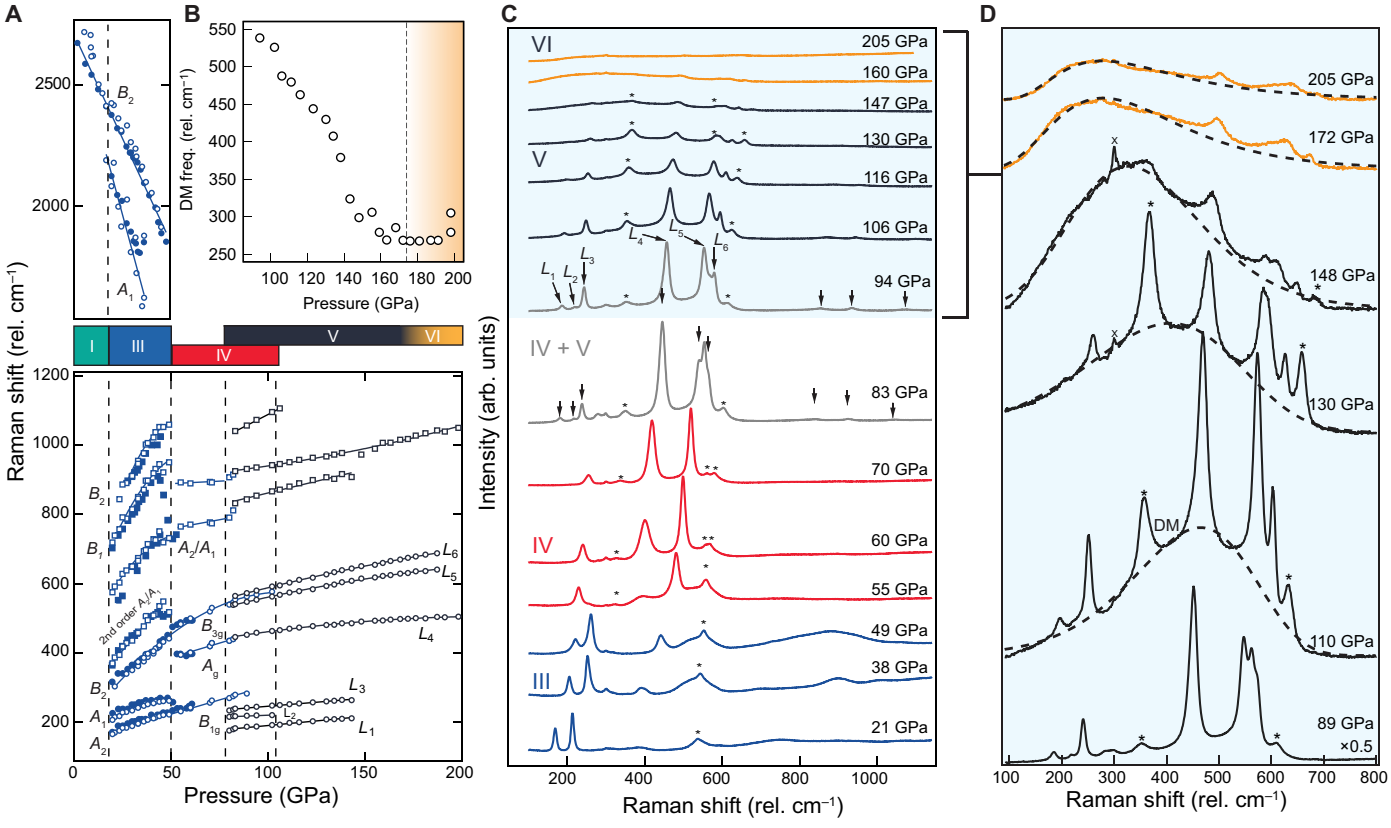

Fig. 1. Raman spectroscopy of HCl. (**A**) Raman frequencies of HCl up to 200 GPa, and the top indicates the symmetric and antisymmetric H—Cl stretch, with their disappearance associated with the symmetrization of the hydrogen bond network. Square markers denote the HCl excitations that are found to be in an energy regime typical of librational movement (*31*). The filled symbols correspond to previous studies (*31*, *32*). (**B**) Pressure dependence of the frequency of the broad disordered mode (DM) highlighted in (D), and dashed line indicates the approximate point of inflection. (**C**) Raman spectra of HCl phases III, IV, and V/VI up to 205 GPa. Stars indicate the excitations due to trace Cl_2 impurities (*47*). (**D**) Selected Raman spectra above 89(10) GPa show that a broad band emerges, which increases in intensity while red shifting with pressure. The dashed black line represents a log-normal excitation profile frequently used in the characterization of the boson peak in disordered systems (*64*).

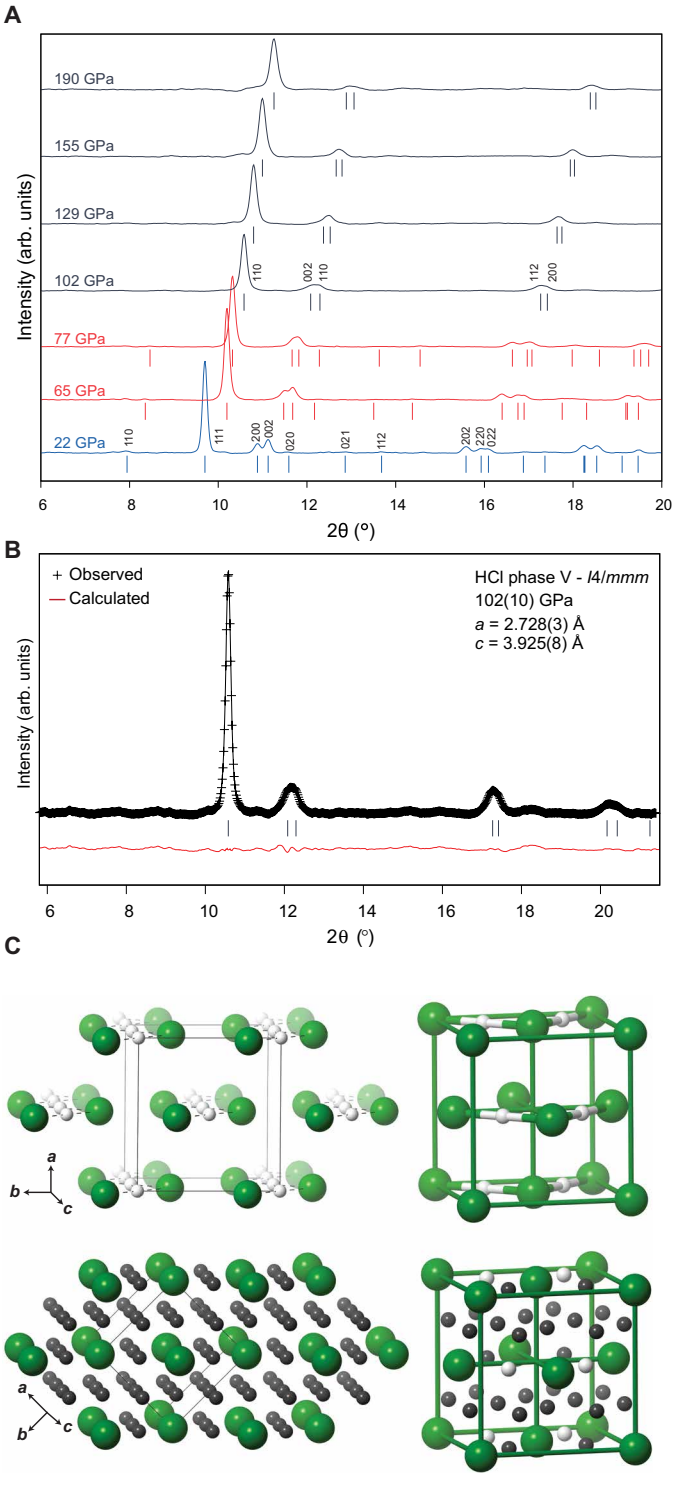

Fig. 2. X-ray diffraction patterns of HCl under pressure. (**A**) Powder diffraction patterns of HCl with increasing pressure (λ = 0.4131 Å). Tick marks show the calculated peak positions, and indices are given for major reflections. Line colors denote phases II, IV, and V following Fig. 1. (**B**) Representative Le Bail refinement of HCl at 102(10) GPa. Experimental data are indicated with points, calculated profile is shown in black, and difference is shown as the lower red trace. Refined unit cell dimensions are $a = 2.728(3)$ and $c = 3.925(8)$ Å. (**C**) Crystal structures of phase IV (top) and phase V (bottom); new disordered H positions are shown in gray. Thin black lines outline unit cells, and thick green lines indicate the approximate fcc unit cell of the chlorine lattice.

agreement with those determined experimentally (fig. S2). In addition, the frequencies generated in a previous numerical study (*35*) show excellent consistency with our measurements for phase III/IV (Fig. 1A).

The transition to the postsymmetrized phase, phase V, occurs in the region 80(10) to 100(10) GPa, where nine additional Raman modes (indicated with arrows in Fig. 1C) emerge and are found to coexist with excitations inherent to phase IV. In the low-frequency region, we assign the Raman modes that are below 650 cm^{-1} as optical lattice modes (L_1 to L_6). Above 800 cm^{-1}, we also observe enhanced Raman activity in a frequency region formerly occupied by librational excitations of the presymmetrized phase III (*32*). Changes in the x-ray diffraction patterns are observed above 90 GPa and are more subtle: The (020) reflection is lost, and the (200) and (002) reflections merge to form one broad peak at ca. $2\theta = 12°$ (Fig. 2A).

Structure searching and molecular dynamics (MD) calculations have suggested two possible phase V structures in space groups $P2_1/m$ (*35*) and $P\bar{1}$ (*34*). However, there is poor agreement between the calculated x-ray diffraction patterns of these predicted structures and our experimental data (fig. S3). Instead, we find the structure of phase V to be tetragonal with unit cell dimensions $a = 2.728(3)$ and $c = 3.925(8)$ Å at 102 GPa. This unit cell is derived by direct distortion of phase IV and provides an excellent fit to the observed data (Fig. 2). The equation of state of HCl is presented in fig. S4; the refined equation of state parameters are as follows: $V_0 = 42.8(10)$ $Å^3$, $K_0 = 5.9(8)$ GPa, and $K_p = 3.91(7)$.

To gain insight into the underlying physics driving the IV-to-V transition, we investigated the behavior of HCl, and in particular the hydrogen atoms, using DFT MD calculations at 95 GPa and ran at temperatures up to 1000 K. Simulations used supercells of both the experimentally determined phase V lattice parameters and those of the calculated phase IV at 95 GPa. Results are very similar for both sets of structures. We find that, under all temperature conditions, Cl atoms retain a solid lattice, in agreement with our x-ray diffraction measurements, that can be understood as an approximately fcc structure. In contrast, the protons' behavior changes qualitatively with temperature: At 625 K and less, protons do not leave the bonds of phase IV, while at 750 K and above, they become mobile. The protons do not move freely through the crystal but hop into the midpoints of all 12 nearest-neighbor Cl—Cl connections, occupying them roughly equally (Fig. 3A). Despite the localized nature of the proton sites [also seen in superionic water (*38*) and water-ammonia mixtures (*39*)], the hopping mechanism leads to macroscopic proton diffusion. The ionic conductivity at 750 K, the onset of hydrogen diffusion, is estimated from the Nernst-Einstein relation to be 9.8 S cm^{-1}, well above the accepted threshold of 1 S cm^{-1} for superionic materials (*40*). The resulting proton disorder, as we discuss below, explains both our x-ray and Raman measurements. Note that we find proton mobility at temperatures much higher than the experimental conditions. However, our calculations did not include nuclear quantum effects, defects, or interfaces and used supercells (108 to 256 molecules) that likely experience superheating; all of which are expected to artificially stabilize the solid against any diffusive state. It is not unlikely that mobile hydrogen can already be present at room temperature in our experiments. For comparison, analogous diffusive hydrogen sublattices simulated in H_2O and NH_3 at similar pressures require higher temperatures of 1700 and 1000 K, respectively, in the simulations but have been detected at temperatures 700 and 300 K lower (*13*, *41*, *42*).

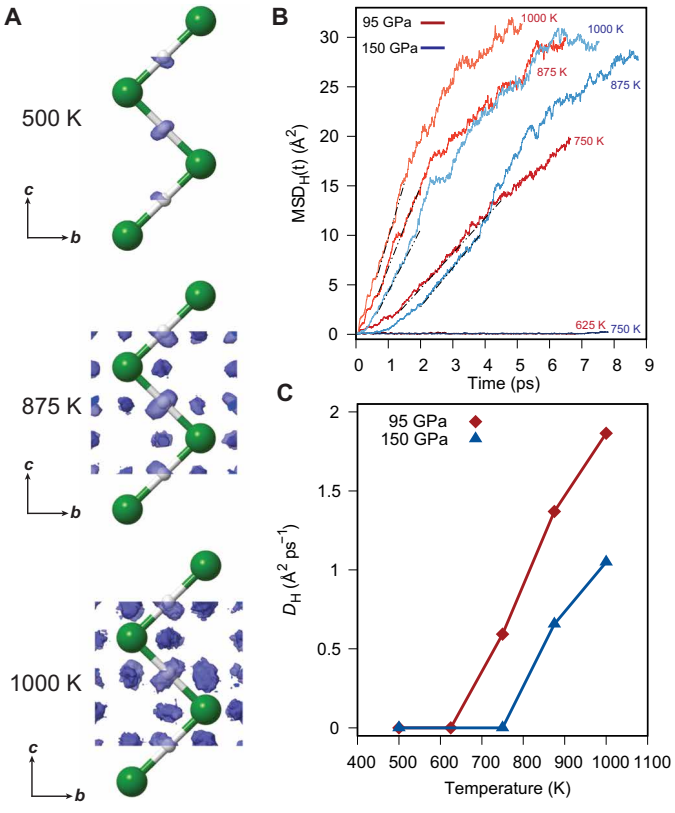

Fig. 3. MD and proton mobility. (**A**) Average proton positions (blue) for phase V at 150 GPa and different temperatures compared to initial geometries (balls and sticks) from DFT MD simulations. From 750 K (at 95 GPa) and above, protons migrate to additional sites lying on Cl···Cl interatomic contacts. (**B**) Proton mean squared displacement $MSD_H(t)$ at 95 GPa (red) and 150 GPa (blue) and different temperatures (500 to 1000 K). Linear fits are indicated with black dashed lines. (**C**) Derived proton diffusion coefficients D_H for HCl with increasing temperature.

The relationship between the ordered (IV) and disordered (V) hydrogen positions can be seen if the underlying Cl sublattice is indeed approximated as an fcc structure (Fig. 2C). In this approximated phase IV, hydrogen atoms occupy 4 of the 24 equivalent 24d Wyckoff sites, giving rise to the zigzagging chains of symmetric hydrogen bonds. In the observed tetragonal structure, the equivalent H atom positions are (1/2, 0, 0, 4*c*) and (1/4, 1/4, 1/4, 8*f*). We propose that transitioning to phase V leads to hydrogen atoms partially occupying all the 24*d* sites with equal probability. Critically, through the occupancy of new hydrogen lattice sites, the local bonding environment of each Cl atom is altered. A notably similar phenomenon was observed in water ice VII above ca. 26 GPa using neutron diffraction (*43*). In this phase, compression leads to increasing partial occupancy of "interstitial void" sites that lie outside the assumed hydrogen bond between oxygen atoms. The appearance of H atoms outside the expected covalent bond was postulated to be due to a relative weakening of the covalent O—H interaction versus hydrogen bond strength. This effect can be seen even more clearly in HCl phase V, as hydrogen bond strength that increases the energetic difference between the covalent "ordered" (white) and "disordered" 24*d* sites (gray) is lowered to the point at which proton migration occurs.

Further support for the emergence of a disordered hydrogen sublattice can be found by comparing the enthalpies of predicted phases. Transitioning to the predicted structures in (*34*, *35*) requires significant distortions in the Cl sublattice that lead to increased packing efficiency as compared to the disordered phase V, as measured by *PV* terms in computed enthalpies. While this might seem to imply that phase V is metastable, DFT inherently fails to capture the contribution of configurational entropy due to proton disorder. A conservative estimate of the entropic contribution, assuming that each Cl atom is bonded to two H atoms, equates to 38 meV per HCl molecule at 300 K. This contribution stabilizes phase V against the predicted structures up to at least 230 GPa, when the $P\bar{1}$ structure (*34*) is more stable than phase IV by 40 meV per HCl. In the absence of this disorder, our own calculations indicate that, in the ground state, phase IV is the thermodynamically most stable phase up to 120 GPa above which the predicted $P\bar{1}$ phase has the lowest enthalpy in agreement with (*34*).

Above 90 GPa, in contrast with the subtle changes observed in x-ray diffraction patterns, the Raman spectra of phase V are seen to undergo profound changes, as seen in Fig. 1C, comparing spectra at 94 and 147 GPa. Intriguingly, these changes are observed primarily to be a consequence of an emergent broad low-frequency excitation (full width at half maximum of ~300 cm^{-1}), illustrated by the black dashed line in Fig. 1D. Typically, broad features in the frequency range of the lattice modes are indicative of structural disorder, hence our designation of "disorder mode(s)" (DM) in Fig. 1D. For example, broad excitations are a defining characteristic in amorphous materials (*44*), where the overall Raman spectrum is found to resemble the vibrational density of states as symmetry restraints are relaxed and optical phonons spanning the Brillouin zone are active. Intuitively, the emergence of this mode in HCl would initially appear to be in contradiction with our diffraction observations, which demonstrate the persistence of a crystalline powder. Upon further compression, this band is found to shift to lower frequencies while increasing in intensity, eventually superseding the well-defined Raman excitations above 148 GPa. Above ca. 175 GPa, the frequency of this excitation plateaus and gradually weakens, becoming difficult to detect above 200 GPa as seen in Fig. 1D.

Correlated to the spectral changes discussed previously, HCl is also found to change in appearance, as seen in the sequential photomicrographs in Fig. 4A. These changes are typical of a pressure-induced optical bandgap closure (*45*–*47*), whereby the absorption edge passes through the visible wavelengths (Fig. 4 and fig. S6). With increasing pressure, it is found that the optical bandgap of HCl (estimated from the absorption edge; fig. S6) reduces with a linear pressure dependence and is extrapolated to close at ca. 240(10) GPa. Above 210 GPa, the sample becomes sufficiently optically dense that no transmission could be detected down to 0.7 eV as seen in Fig. 4B. Curiously, a significant change is found between pressures of 164(10) and 180(10) GPa, where an abrupt drop in the transmission above 1200 nm, seen in fig. S6B, results in a steep rise in the absorbance, reaching our detection limit (~2 optical density), and shifts to higher energies as a function of pressure (Fig. 4A). The energy range of this feature (0.8 to 1 eV) is characteristic of intraband excitations and therefore could be explained as an absorption due to free charge carriers populating the conduction band. Additional techniques such as in situ four-probe electrical measurements or optical reflectivity would greatly enhance our understanding of the conductive properties of HCl (*48*–*50*); however, this compound poses significant technical

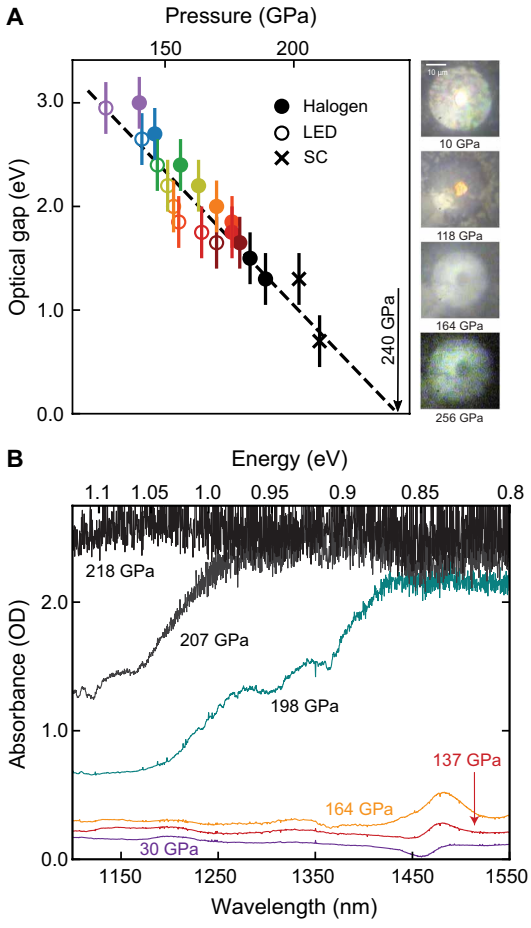

Fig. 4. Optical absorption under pressure. (**A**) Left: Optical bandgap measurements, estimated from the absorption edge (see fig. S7), using various broadband light sources as a function of pressure. The dashed black line is a linear fit that indicates that the optical bandgap will close at around 240(10) GPa. Right: Sequential microphotographs of the HCl sample chamber from 10 to 256 GPa; the sample appears darker and redder with pressure as shorter wavelength light becomes attenuated. SC, supercontinuum. (**B**) Absorbance spectrum over the shortwave IR range. A large increase in absorbance is found between 164 and 198 GPa below 1.1 eV, indicative of free-charge carriers populating the conduction band. No detectable transmission was observed above 210 GPa down to 1700 nm, suggesting that the bandgap is less than 0.7 eV. OD, optical density; LED, light-emitting diode.

challenges because of the cryogenic loading technique and its highly reactive and corrosive nature. Therefore, although HCl has not become fully metallic above 160 GPa, it may exhibit a degree of conductivity before it fully metallizes at 240(10) GPa.

At approximately 170 GPa, we define the complete transformation to phase VI, which was found to sluggishly transform over an 80-GPa interval. We characterize this phase as a high-pressure modification of phase V and having the following observable characteristics: a crystalline chlorine sublattice and disordered vibrational properties. As mentioned previously, initially, it would appear that these characteristics are incompatible; however, it is important to note that the x-ray diffraction is sensitive only to the chlorine positions, having a negligible contribution from hydrogen. Therefore, to explain the inherent disorder captured in our Raman measurements, we again turn to our first-principles calculations to elucidate the role of hydrogen in phase VI. Further simulations were carried out at 150 GPa following the same methodology; the resulting proton mean squared displacement and derived diffusion coefficients at both 95 and 150 GPa are shown in Fig. 3 (B and C). It is seen that the simulations at 150 GPa require significantly higher temperatures, in excess of 850 K, to induce comparable proton diffusion, indicating that proton mobility becomes increasingly inhibited upon compression above 100 GPa. Similar behavior in population exchanges of mobile/immobile hydrogen has been recently reported in an analogous system, high-pressure water ice, using proton nuclear magnetic resonance (*51*). In addition, in this study, it was also found that the nuclear quantum effects lead to far greater mobility of hydrogen-bonded protons than indicated by calculations, a result supported by recent DFT calculations (*52*).

In summary, we find that HCl resists decomposition up to pressures in excess of 250 GPa and find no evidence for the previously predicted candidate structures. Instead, we identify a new phase, phase V (space group *I*4/*mmm*), characterized by the reintroduction of configurational disorder as protons become mobilized, via a hopping mechanism, to new lattice sites. Upon further compression, we observe the gradual transformation to phase VI, distinguishable from phase V by exhibiting disordered vibrational characteristics and a strong absorption in the near IR, likely due to the presence of free charge carriers. Through MD calculations, this transition is found to be correlated and therefore suggested to be motivated by the reduction of proton mobility with pressure. Ultimately, we find that, even at densities far surpassing hydrogen bond symmetrization, phases are still found to be characterized by the physics of the hydrogen atoms. These findings raise intriguing questions about the nature of hydrogen bonding and superionicity in materials at ultrahigh pressures. Current theoretical approaches struggle to describe disordered systems, and it may be that quantum nuclear effects play a far greater role in hydrogen-bonded systems at high densities than previously thought, having implications for hydrogen-rich matter under conditions of extreme temperature and pressures, such as planetary mantles.

MATERIALS AND METHODS

Experimental procedures

We have studied the behavior of pure HCl up to pressures of 260 GPa in diamond anvil cells (DACs) by x-ray diffraction and Raman spectroscopy. Flat culet diamonds (200 μm) were used for x-ray diffraction experiments under 60 GPa, while 30-μm culets were used for higher-pressure Raman spectroscopy experiments. Rhenium foil is inert to HCl and was used as the gasket material in all experiments (*32*). Solid HCl (99.9% purity) was cryogenically loaded into a DAC under a dry nitrogen atmosphere. Successful loading was confirmed by Raman spectroscopy.

Excitation wavelengths of 532 and 660 nm were used for Raman spectroscopy measurements using a custom-built confocal microfocused Raman system. Pressure was determined through both ruby fluorescence ($P < 100$ GPa) and the Raman edge of stressed diamond correlated to the equation of state of a tungsten pressure marker (*53*).

Absorbance was estimated through transmission spectroscopy in the visible range using a black-body spectrum broadband halogen and light-emitting diode light sources (between ~400 and 1000 nm) with a charge-coupled device (CCD) sensitive to the visible. Absorbance in the IR range (between ~800 and 1800 nm) was measured

using a supercontinuum laser using the appropriate InGaAs CCD detector, which is sensitive in the IR regime.

Angle-dispersive x-ray diffraction patterns were recorded on a fast image plate detector with synchrotron radiation (λ = 0.4141 Å, 30 keV) at beamline BL10XU, SPring-8, Japan (*54*). Two-dimensional image plate data were integrated with DIOPTAS (*55*) to yield intensity versus 2θ plots. Le Bail (*56*) profile refinements were carried out in Jana2006 (*57*). Volume and linear equation of state parameters were determined using EoSFit 7 (*58*).

Ab initio calculations

DFT calculations were performed with the Vienna Ab initio Simulation Package (VASP) using plane wave basis sets (cutoff energy E_c = 800 eV) in conjunction with projector augmented wave (PAW) datasets (cutoff radii $r_{c,O} = 1.5a_B$, $r_{c,H} = 0.8a_B$) (*59*, *60*). Structural optimizations and MD simulations used the dispersion-corrected optB88-vdW exchange-correlation functional (*61*, *62*); the lattice constants of phases III and IV were very similar when using the semilocal Perdew-Burke-Ernzerhof (PBE) functional. Brillouin zone linear sampling rates were $2\pi \times 0.025$ Å^{-1} for optimizations ($2\pi \times 0.05$ Å^{-1} for MD). MD simulations used 108-molecule supercells starting from both phase IV (calculated) and phase V (experimental) lattice parameters at 95 and 150 GPa. Tests with 256-molecule supercells showed no discernible difference in diffusion behavior (fig. S8). Simulations used a 0.5-fs time step and a Nosé thermostat (*63*), were equilibrated for 0.5 ps, and ran for up to 8.5 ps.

SUPPLEMENTARY MATERIALS

Supplementary material for this article is available at https://science.org/doi/10.1126/sciadv.abi9507

REFERENCES AND NOTES

1. A. Janotti, C. G. Van De Walle, Hydrogen multicentre bonds. *Nat. Mater.* **6**, 44–47 (2007).
2. C. J. Sahle, C. Sternemann, C. Schmidt, S. Lehtola, S. Jahn, L. Simonelli, S. Huotari, M. Hakala, T. Pylkkänen, A. Nyrow, K. Mende, M. Tolan, K. Hämäläinen, M. Wilke, Microscopic structure of water at elevated pressures and temperatures. *Proc. Natl. Acad. Sci. U.S.A.* **110**, 6301–6306 (2013).
3. B. Santra, J. Klimes, D. Alfe, A. Tkatchenko, B. Slater, A. Michaelides, R. Car, M. Scheffler, Hydrogen bonds and van der Waals forces in ice at ambient and high pressures. *Phys. Rev. Lett.* **107**, 185701 (2011).
4. E. Schwegler, G. Galli, F. Gygi, Water under pressure. *Phys. Rev. Lett.* **84**, 2429–2432 (2000).
5. V. Naden Robinson, Y. Wang, Y. Ma, A. Hermann, Stabilization of ammonia-rich hydrate inside icy planets. *Proc. Natl. Acad. Sci. U.S.A.* **114**, 9003–9008 (2017).
6. A. F. Goncharov, V. V. Struzhkin, M. S. Somayazulu, R. J. Hemley, H. K. Mao, Compression of ice to 210 gigapascals: Infrared evidence for a symmetric hydrogen-bonded phase. *Science* **273**, 218–220 (1996).
7. P. Loubeyre, R. LeToullec, E. Wolanin, M. Hanfland, D. Hausermann, Modulated phases and proton centring in ice observed by x-ray diffraction up to 170 GPa. *Nature* **397**, 503–506 (1999).
8. O. Mishima, L. D. Calvert, E. Whalley, An apparently first-order transition between two amorphous phases of ice induced by pressure. *Nature* **314**, 76–78 (1985).
9. Y. Q. Cai, H.-K. Mao, P. C. Chow, J. S. Tse, Y. Ma, S. Patchkovskii, J. F. Shu, V. Struzhkin, R. J. Hemley, H. Ishii, C. C. Chen, I. Jarrige, C. T. Chen, S. R. Shieh, E. P. Huang, C. C. Kao, Ordering of hydrogen bonds in high-pressure low-temperature H_2O. *Phys. Rev. Lett.* **94**, 025502 (2005).
10. I. Errea, M. Calandra, C. J. Pickard, J. R. Nelson, R. J. Needs, Y. Li, H. Liu, Y. Zhang, Y. Ma, F. Mauri, Quantum hydrogen-bond symmetrization in the superconducting hydrogen sulfide system. *Nature* **532**, 81–84 (2016).
11. X. Huang, X. Wang, D. Duan, B. Sundqvist, X. Li, Y. Huang, H. Yu, F. Li, Q. Zhou, B. Liu, T. Cui, High-temperature superconductivity in sulfur hydride evidenced by alternating-current magnetic susceptibility. *Natl. Sci. Rev.* **6**, 713–718 (2019).
12. E. J. Pace, X.-D. Liu, P. Dalladay-Simpson, J. Binns, M. Peña-Alvarez, J. P. Attfield, R. T. Howie, E. Gregoryanz, Properties and phase diagram of $(H_2S)_2H_2$. *Phys. Rev. B* **101**, 174511 (2020).
13. C. Cavazzoni, G. L. Chiarotti, S. Scandolo, E. Tosatti, M. Bernasconi, M. Parrinello, Superionic and metallic states of water and ammonia at giant planet conditions. *Science* **238**, 44–46 (1999).
14. M. Gauthier, P. Pruzan, J. C. Chervin, J. M. Besson, Raman scattering study of ammonia up to 75 GPa: Evidence for bond symmetrization at 60 GPa. *Phys. Rev. B* **37**, 2102–2115 (1988).
15. J. L. Finney, D. T. Bowron, A. K. Soper, T. Loerting, E. Mayer, A. Hallbrucker, Structure of a New dense amorphous ice. *Phys. Rev. Lett.* **89**, 205503 (2002).
16. C. J. Pickard, R. J. Needs, Highly compressed ammonia forms an ionic crystal. *Nat. Mater.* **7**, 775–779 (2008).
17. M. Benoit, M. Bernasconi, P. Focher, M. Parrinello, New high-pressure phase of ice. *Phys. Rev. Lett.* **76**, 2934–2936 (1996).
18. Y. Wang, H. Liu, J. Lv, L. Zhu, H. Wang, Y. Ma, High pressure partially ionic phase of water ice. *Nat. Commun.* **2**, 563–565 (2011).
19. A. Hermann, N. W. Ashcroft, R. Hoffmann, High pressure ices. *Proc. Natl. Acad. Sci.* **109**, 745–750 (2011).
20. B. Militzer, H. F. Wilson, New phases of water ice predicted at megabar pressures. *Phys. Rev. Lett.* **105**, 195701 (2010).
21. M. Guthrie, R. Boehler, J. J. Molaison, B. Haberl, A. M. Dos Santos, C. Tulk, Structure and disorder in ice VII on the approach to hydrogen-bond symmetrization. *Phys. Rev. B* **99**, 184112 (2019).
22. N. Nettelmann, R. Helled, J. J. Fortney, R. Redmer, New indication for a dichotomy in the interior structure of Uranus and Neptune from the application of modified shape and rotation data. *Planet. Space Sci.* **77**, 143–151 (2013).
23. J. J. Lissauer, D. C. Fabrycky, E. B. Ford, W. J. Borucki, F. Fressin, G. W. Marcy, J. A. Orosz, J. F. Rowe, G. Torres, W. F. Welsh, N. M. Batalha, S. T. Bryson, L. A. Buchhave, D. A. Caldwell, J. A. Carter, D. Charbonneau, J. L. Christiansen, W. D. Cochran, J.-M. Desert, E. W. Dunham, M. N. Fanelli, J. J. Fortney, T. N. Gautier III, J. C. Geary, R. L. Gilliland, M. R. Haas, J. R. Hall, M. J. Holman, D. G. Koch, D. W. Latham, E. Lopez, S. McCauliff, N. Miller, R. C. Morehead, E. V. Quintana, D. Ragozzine, D. Sasselov, D. R. Short, J. H. Steffen, A closely packed system of low-mass, low-density planets transiting Kepler-11. *Nature* **470**, 53–58 (2011).
24. A. S. J. Méndez, F. Trybel, R. J. Husband, G. Steinle-Neumann, H. P. Liermann, H. Marquardt, Bulk modulus of H_2O across the ice VII-ice X transition measured by time-resolved x-ray diffraction in dynamic diamond anvil cell experiments. *Phys. Rev. B* **103**, 064104 (2021).
25. E. Sándor, R. F. C. Farrow, Crystal structure of solid hydrogen chloride and deuterium chloride. *Nature* **213**, 171–172 (1967).
26. E. Sándor, M. W. Johnson, Crystal structure and the lower phase transition in solid deuterium bromide. *Nature* **217**, 541–543 (1968).
27. M. W. Johnson, E. Sándor, E. Arzi, The crystal structure of deuterium fluoride. *Acta Crystallogr. Sect. B* **31**, 1998–2003 (1975).
28. A. Ikram, B. H. Torrie, B. M. Powell, Structures of solid deuterium bromide and deuterium iodide. *Mol. Phys.* **79**, 1037–1049 (1993).
29. E. Katoh, H. Yamawaki, H. Fujihisa, M. Sakashita, K. Aoki, Raman and infrared study of phase transitions in solid HBr under pressure. *Phys. Rev. B* **59**, 11244–11250 (1999).
30. J. Binns, X.-D. Liu, P. Dalladay-Simpson, V. Afonina, E. Gregoryanz, R. T. Howie, Synthesis and stability of hydrogen iodide at high pressures. *Phys. Rev. B.* **96**, 144105 (2017).
31. K. Aoki, E. Katoh, H. Yamawaki, M. Sakashita, H. Fujihisa, Hydrogen-bond symmetrization and molecular dissociation in hydrogen halids. *Phys. B Condens. Matter.* **265**, 83–86 (1999).
32. E. Katoh, H. Yamawaki, H. Fujihasa, M. Sakashita, K. Aoki, Raman study of phase transition and hydrogen bond symmetrization in solid DCl at high pressure. *Phys. Rev. B.* **61**, 119–124 (2000).
33. H. Shimizu, K. Kamabuchi, T. Kume, S. Sasaki, High-pressure elastic properties of the orientationally disordered and hydrogen-bonded phase of solid HCl. *Phys. Rev. B* **59**, 11727–11732 (1999).
34. L. Zhang, Y. Wang, X. Zhang, Y. Ma, High-pressure phase transitions of solid HF, HCl, and HBr: An ab initio evolutionary study. *Phys. Rev. B* **82**, 014108 (2010).
35. D. Duan, F. Tian, Z. He, X. Meng, L. Wang, C. Chen, X. Zhao, B. Liu, T. Cui, Hydrogen bond symmetrization and superconducting phase of HBr and HCl under high pressure: An ab initio study. *J. Chem. Phys.* **133**, 074509 (2010).
36. C. Chen, Y. Xu, X. Sun, S. Wang, Novel superconducting phases of HCl and HBr under high pressure: An Ab initio study. *J. Phys. Chem. C* **119**, 17039–17043 (2015).
37. F. Datchi, S. Ninet, M. Gauthier, A. M. Saitta, B. Canny, F. Decremps, Solid ammonia at high pressure: A single-crystal x-ray diffraction study to 123 GPa. *Phys. Rev. B Condens. Matter Mater. Phys.* **73**, 1741115 (2006).
38. J.-A. Hernandez, R. Caracas, Superionic-superionic phase transitions in body-centered cubic H_2O ice. *Phys. Rev. Lett.* **117**, 135503 (2016).

39. V. Naden Robinson, A. Hermann, Plastic and superionic phases in ammonia–water mixtures at high pressures and temperatures. *J. Phys. Condens. Matter* **32**, 184004 (2020).
40. J. B. Boyce, B. A. Huberman, Superionic conductors: Transitions, structures, dynamics. *Phys. Rep.* **51**, 189–265 (1979).
41. A. F. Goncharov, N. Goldman, L. E. Fried, J. C. Crowhurst, I.-F. W. Kuo, C. J. Mundy, J. M. Zaug, Dynamic ionization of water under extreme conditions. *Phys. Rev. Lett.* **94**, 125508 (2005).
42. S. Ninet, F. Datchi, A. M. Saitta, Proton disorder and superionicity in hot dense ammonia ice. *Phys. Rev. Lett.* **108**, 165702 (2012).
43. M. Guthrie, R. Boehler, C. A. Tulk, J. J. Molaison, A. M. dos Santos, K. Li, R. J. Hemley, Neutron diffraction observations of interstitial protons in dense ice. *Proc. Natl. Acad. Sci. U.S.A.* **110**, 10552–10556 (2013).
44. R. J. Hemley, H. K. Mao, P. M. Bell, B. O. Mysen, Raman spectroscopy of SiO_2 glass at high pressure. *Phys. Rev. Lett.* **57**, 747–750 (1986).
45. S. Desgreniers, Y. K. Vohra, A. L. Ruoff, Optical response of very high density solid oxygen to 132 GPa. *J. Phys. Chem.* **94**, 1117–1122 (1990).
46. M. I. Eremets, R. J. Hemley, H. K. Mao, E. Gregoryanz, Semiconducting non-molecular nitrogen up to 240 GPa and its low-pressure stability. *Nature* **411**, 170–174 (2001).
47. P. Dalladay-Simpson, J. Binns, M. Peña-Alvarez, M.-E. Donnelly, E. Greenberg, V. Prakapenka, X.-J. Chen, E. Gregoryanz, R. T. Howie, Band gap closure, incommensurability and molecular dissociation of dense chlorine. *Nat. Commun.* **10**, 1134 (2019).
48. M. Hou, Y. He, B. G. Jang, S. Sun, Y. Zhuang, L. Deng, R. Tang, J. Chen, F. Ke, Y. Meng, V. B. Prakapenka, B. Chen, J. H. Shim, J. Liu, D. Y. Kim, Q. Hu, C. J. Pickard, R. J. Needs, H. K. Mao, Superionic iron oxide–hydroxide in Earth's deep mantle. *Nat. Geosci.* **14**, 174–178 (2021).
49. M. I. Eremets, I. A. Troyan, Conductive dense hydrogen. *Nat. Mater.* **10**, 927–931 (2011).
50. G. Rillo, M. A. Morales, D. M. Ceperley, C. Pierleoni, Optical properties of high-pressure fluid hydrogen across molecular dissociation. *Proc. Natl. Acad. Sci. U.S.A.* **116**, 9770–9774 (2019).
51. T. Meier, S. Petitgirard, S. Khandarkhaeva, L. Dubrovinsky, Observation of nuclear quantum effects and hydrogen bond symmetrisation in high pressure ice. *Nat. Commun.* **9**, 2766 (2018).
52. F. Trybel, M. Cosacchi, T. Meier, V. M. Axt, G. Steinle-Neumann, Proton dynamics in high-pressure ice-VII from density functional theory. *Phys. Rev. B* **102**, 184310 (2020).
53. Y. Akahama, H. Kawamura, Pressure calibration of diamond anvil Raman gauge to 410 GPa. *J. Phys. Conf. Ser.* **215**, 12195 (2010).
54. Y. Ohishi, N. Hirao, N. Sata, K. Hirose, M. Takata, Highly intense monochromatic X-ray diffraction facility for high-pressure research at SPring-8. *High Press. Res.* **28**, 163–173 (2008).
55. C. Prescher, V. B. Prakapenka, *DIOPTAS*: A program for reduction of two-dimensional x-ray diffraction data and data exploration. *High Press. Res.* **35**, 223–230 (2015).
56. A. Le Bail, H. Duroy, J. L. Fourquet, Ab-initio structure determination of LiSbWO6 by X-ray powder diffraction. *Mater. Res. Bull.* **23**, 447–452 (1988).
57. V. Petříček, M. Dušek, L. Palatinus, Crystallographic computing system JANA2006: General features. *Zeitschrift für Krist. Mater.* **229**, 345–352 (2014).
58. J. Gonzalez-Platas, M. Alvaro, F. Nestola, R. J. Angel, *EosFit7-GUI*: A new graphical user interface for equation of state calculations, analyses and teaching. *J. Appl. Cryst.* **49**, 1377–1382 (2016).
59. G. Kresse, F. Furthmüller, Efficient iterative schemes for ab initio total-energy calculations using a plane-wave basis set. *Phys. Rev. B* **54**, 11169–11186 (1996).
60. G. Kresse, D. Joubert, From ultrasoft pseudopotentials to the projector augmented-wave method. *Phys. Rev. B* **59**, 1758–1775 (1999).
61. J. Klimeš, D. R. Bowler, A. Michaelides, Chemical accuracy for the van der Waals density functional. *J. Phys. Condens. Matter* **22**, 022201 (2010).
62. J. Klimeš, D. R. Bowler, A. Michaelides, Van der Waals density functionals applied to solids. *Phys. Rev. B* **83**, 195131 (2011).
63. S. Nosé, A unified formulation of the constant temperature molecular dynamics methods. *J. Chem. Phys.* **81**, 511–519 (1984).
64. W. Schirmacher, G. Diezemann, C. Ganter, Harmonic vibrational excitations in disordered solids and the "Boson Peak". *Phys. Rev. Lett.* **81**, 136–139 (1998).

Acknowledgments

Funding: P.D.-S. and R.T.H. acknowledge their respective "1000 Young Talents" awards and the "Top 1000 Talents" award of H.-K. Mao. R.T.H. acknowledges that part of this research was supported by the National Natural Science Foundation of China (NSFC) project no. 11974034. M.P.-A. acknowledges the support of the European Research Council (ERC) Grant Hecate reference no. 695527 secured by G. Ackland and FLF Award - MR/T043733/1. Parts of this research were also conducted at the SPring-8 facility under proposal no. 2017A1401. Computational resources provided by the U.K.'s National Supercomputer Service through the U.K. Car-Parrinello consortium (EPSRC grant no. EP/P022561/1) and by the U.K. Materials and Molecular Modelling Hub (no. EP/P020194) are acknowledged. **Author contributions:** J.B., E.G., R.T.H., and P.D.-S. designed the study and experiments. A.H. carried out simulation work. J.B., M.P.-A., M.-E.D., M.W., S.I.K., E.G., R.T.H., and P.D.-S. performed the experiments. J.B., A.H., and P.D.-S. analyzed experimental and simulation data. J.B., A.H., E.G., R.T.H., and P.D.-S. wrote the manuscript with input from all authors. **Competing interests:** The authors declare that they have no competing interests. **Data and materials availability:** All data needed to evaluate the conclusions in the paper are present in the paper and/or the Supplementary Materials.

Submitted 11 April 2021
Accepted 21 July 2021
Published 1 September 2021
10.1126/sciadv.abi9507

Citation: J. Binns, A. Hermann, M. Peña-Alvarez, M.-E. Donnelly, M. Wang, S. I. Kawaguchi, E. Gregoryanz, R. T. Howie, P. Dalladay-Simpson, Superionicity, disorder, and bandgap closure in dense hydrogen chloride. *Sci. Adv.* **7**, eabi9507 (2021).